Research Article

Eman Aldosari, Mohamed Rabia*, Qinfang Zhang, and Hissah Hamad Altilasi

Single-step fabrication of Mn(IV) oxide-Mn(II) sulfide/poly-2-mercaptoaniline porous network nanocomposite for pseudo-supercapacitors and charge storage

https://doi.org/10.1515/phys-2025-0132
received October 15, 2024; accepted February 24, 2025

Abstract: The single-step fabrication of the Mn(IV) oxide-Mn(II) sulfide/Poly-2-mercaptoaniline porous network nanocomposite (MnO_2-MnS/P2MA) involves incorporating the Mn source into the P2MA polymer during polymerization. XPS analysis confirms the presence of peaks corresponding to Mn(IV) and Mn(II), while XRD analysis highlights the formation of pronounced crystalline peaks, indicative of excellent semiconductive properties, with a crystalline size of 42 nm. The nanocomposite serves as the main electrode for electrochemically assessing its charge storage capabilities. Optimal energy density (E) values are achieved at lower current densities, with 9.7 and 7.0 W h/kg at 0.6 and 1.0 A/g, respectively. Similarly, the specific capacitance (C_S) reaches peak values of 120 and 86 F/g within the same current density range. The electrochemical impedance spectroscopy (EIS) behavior is notable, with an R_s value of 7.3 Ω and an impressive cycle retention of 99.2% over 1,000 cycles. The combination of simple one-pot fabrication, excellent charge storage performance, and high stability underscores the potential of these materials for charge storage applications. The MnO_2-MnS/P2MA nanocomposite's superior EIS behavior, optimal energy and capacitance values, and remarkable cycle stability make it a promising candidate for efficient and reliable charge storage solutions.

*** Corresponding author: Mohamed Rabia**, Nanomaterials Science Research Laboratory, Chemistry Department, Faculty of Science, Beni-Suef University, Beni-Suef, 62514, Egypt,
e-mail: mohamedchem@science.bsu.edu.eg
Eman Aldosari: Department of Chemistry, College of Science, King Saud University, P. O. Box 145111, Riyadh, Saudi Arabia,
e-mail: ialdowsary@KSU.EDU.SA
Qinfang Zhang: School of Materials Science and Engineering, Yancheng Institute of Technology, Yancheng, China
Hissah Hamad Altilasi: Department of Chemistry, College of Science, King Saud University, P. O. Box 145111, Riyadh, Saudi Arabia

Keywords: poly-2-mercapto aniline, Mn(IV) oxide-Mn(II) sulfide, supercapacitors, charge storage

1 Introduction

The growing energy crisis and diminishing fossil fuel reserves have heightened the development of sustainable and renewable energy sources. To utilize these energy sources efficiently, various energy-harvesting technologies are required. In addition to capturing energy, it is equally important to have effective energy storage systems that can store the electricity generated from regenerative materials. One promising approach for energy storage is through electrochemical means. Devices used in electrochemical energy storage are not only more environmentally friendly but also offer a practical solution for modern energy needs [1–3].

Electrochemical energy storage technologies, such as batteries and supercapacitors, are gaining attention due to their high energy density and exceptional cycle efficiency. The ability to quickly charge and discharge these systems is crucial for highly technology applications such as electric vehicles and spacecraft. Among these technologies, supercapacitors stand out because they can deliver rapid energy release and have excellent charge-discharge rates, making them ideal for applications that require quick bursts of power [4,5]. Supercapacitors, in particular, have drawn significant interest due to their ability to deliver rapid acceleration in the performance of storage devices, in which the produced power density allows for quick charging and long-time discharging, which is a valuable trait for many energy applications. Furthermore, their superior cycle life means a sustainable and long-term energy storage solution [6,7].

The advancement of nanostructured materials for supercapacitors has become a significant area of focus in

many research initiatives. Nanostructured metal oxides are of particular interest due to their varied crystallographic structures and the ability to undergo redox reactions, making them valuable in electrochemical energy storage devices. Their unique properties enable them to play a crucial role in enhancing the efficiency and capacity of energy storage systems [8].

Among the different materials being explored, transition metal oxides and hydroxides are prominent choices for supercapacitor electrodes. Some widely used examples include MnO_2, $Co(OH)_2$, and vanadium pentoxide (V_2O_5), each of which has been extensively employed to improve the specific power density and capacitance of supercapacitors. These materials' electrochemical properties allow for more efficient energy storage and conversion, which is essential for applications requiring rapid charge and discharge cycles. One material that stands out for its energy storage capabilities is manganese oxide-sulfide, which exhibits exceptional electrical charge storage behavior [9]. This material benefits from the synergetic effect of the metal oxide and sulfide, resulting in enhanced electrical conductivity and superior electrochemical performance. The combination of manganese oxide's high theoretical capacitance and the sulfide component's ability to facilitate fast redox reactions significantly improves the material's overall charge storage capacity.

The utilization of these nanostructured materials is a key factor in the development of supercapacitors with higher energy densities and longer lifespans. The morphology and nanoscale structure of the metal oxides directly influence their electrochemical performance, as smaller particle sizes and higher surface areas allow for more efficient charge transfer and storage. Researchers are continually working on optimizing these properties through various synthesis techniques and material modifications to achieve even better results.

Overall, the exploration of nanostructured metal oxides and their derivatives, such as oxides and hydroxides of transition metals, has led to substantial progress in supercapacitors progress. By leveraging the distinctive properties of materials like MnO_2, $Co(OH)_2$, V_2O_5, and manganese oxide-sulfide, significant improvements in power density, capacitance, and cycle stability have been realized [10,11]. As research continues, these advancements are expected to drive the development of next-generation energy storage devices for sustainable and high-performance energy solutions.

The use of metal oxides in supercapacitor applications has been validated through various studies focusing on charge storage evaluation. For instance, the C_S values for ZnO and $Ni(OH)_2$ have been estimated at 61.7 and 20.5 F/g, respectively [12,13], when applied to supercapacitors. These findings illustrate the effectiveness of metal oxides in enhancing energy storage capabilities. Alternatively, some research approaches determine charge storage by measuring discharge times, revealing that materials like nickel oxide (NiO), titanium dioxide (TiO_2), and cerium oxide (CeO_2) demonstrate discharge times of 10, 5, and 20 s, respectively [14–16]. These measurements further emphasize the potential of metal oxides in energy storage applications.

Incorporating conjugated polymers has also shown promise in supercapacitor development by facilitating charge transfer and expanding composite material formation with metal oxides. A notable example is polyaniline-co-piperazine, which achieves a C_S of 126 F/g [17]. Also, It was found that a polypyrrole/polyvinyl alcohol composite yielded a C_S of 13 F/g, showcasing the diverse capabilities of polymer-based materials in supercapacitor technology [18]. Similarly, a device utilizing a PEDOT/LiTFSI-PVA composite achieved a C_S of 44 F/g, further underscoring the potential of combining polymers with other materials to enhance performance [19]. Despite these advancements, there is still a need for more accurate estimations of storage efficiency and discharge times, as well as the development of more cost-effective fabrication techniques. Current supercapacitor materials vary in performance, and optimizing these devices for higher efficiency remains a challenge. To address these limitations, the integration of additional composite materials is necessary to achieve greater capacitance. Thiophene-based materials, in particular, offer significant promise when used in conjunction with other oxides and sulfides. These materials could play a crucial role in further improving the charge storage properties of supercapacitors.

In this study, MnO_2-MnS/P2MA nanocomposite is synthesized using a one-pot approach. The material's nanoscale crystalline framework, large-scale production capability, simple fabrication process, and porous structure contribute to its suitability for charge storage applications. To evaluate its electrochemical performance, the nanocomposite serves as the working electrode in a three-electrode cell configuration. Cyclic voltammetry and discharge curve analyses assess its charge storage behavior. The obtained values for P, E, C_S, and EIS, and cyclic stability highlight its outstanding charge storage efficiency. The synergistic effects of MnO_2 and MnS enhance the overall electrochemical properties of the composite, improving charge transfer kinetics and increasing active sites for ion diffusion. Additionally, the P2MA polymer matrix provides mechanical stability and facilitates ion transport, further optimizing the electrode's performance. The porous structure enhances electrolyte penetration, ensuring efficient charge storage and retention. The material exhibits remarkable cyclic stability, retaining its performance over multiple

charge–discharge cycles. This stability, combined with high specific capacitance and superior charge storage capabilities, underscores the potential of MnO_2-MnS/P2MA for next-generation energy storage devices.

2 Experimental

2.1 Materials

2-Mercptoaniline (99.9%, Merck, Germany), potassium permanganate ($KMnO_4$, 99.8%, Pio-Chem, Egypt), hydrochloric acid (HCl, 36%, Pio-Chem), Na_2SO_4 (99.9%, Pio-Chem), Nafion (99.9%, Sigma Aldrich, USA), graphitic powder (99.8%, Pio-Chem), and ethanol (99.9%, Pio-Chem).

2.2 Synthesizing of MnO_2-MnS/P2MA PN nanocomposite

The synthesis of the MnO_2-MnS/P2MA PN nanocomposite is achieved through a one-pot technique that estimates the oxidation of 2-mercaptoaniline using $KMnO_4$ as the oxidant. During this oxidation process, the resulting P2MA polymer is doped with the residues of oxidation, MnO_2 and MnS, which become incorporated into the polymer network. This procedure begins by dissolving 0.06 M of 2-mercaptoaniline in 12 ml of HCl under vigorous stirring to ensure thorough mixing. Concurrently, $KMnO_4$ is dissolved in distilled water to prepare the oxidant solution.

The reaction proceeds with the sudden addition of the $KMnO_4$ solution into the 2-mercaptoaniline solution. This prompt addition triggers the oxidation process, which not only converts the monomer into the polymer but also facilitates the integration of MnO_2 and MnS into the polymer matrix. These inorganic components are distributed within the polymer network, endowing the composite with enhanced chemical and electrical properties that are beneficial for charge storage applications.

The one-pot synthesis method is efficient in creating a nanocomposite where the polymer matrix is simultaneously formed and doped with the MnO_2 and MnS particles. This integration is crucial as it imparts the composite with a synergistic combination of the polymer's flexibility and the inorganic materials' conductivity and electrochemical stability. The presence of MnO_2 and MnS within the P2MA polymer enhances the overall performance of the composite, particularly in applications related to energy storage.

The resulting MnO_2-MnS/P2MA PN nanocomposite exhibits improved electrical conductivity and electrochemical properties due to the distributed MnO_2 and MnS particles within the polymer network. These properties are essential for efficient charge storage, making the composite an effective material for supercapacitor storage devices. The method's simplicity and effectiveness in incorporating these inorganic materials into the polymer structure highlight its potential for large-scale production and application in advanced energy storage technologies.

2.3 The fabrication of pseudo-supercapacitor based on MnO_2-MnS/P2MA PN nanocomposite and the electrochemical study

To fabricate a pseudo-supercapacitor based on the MnO_2-MnS/P2MA PN nanocomposite, the composite is prepared as a paste and cast onto a carbon sheet (0.5 mm thick), which serves as the main electrode in a three-electrode cell. To create a homogeneous paste, the composite is dispersed in 5.0 mg of graphite powder, 0.1 ml Nafion, and 0.75 ml ethanol. This mixture is stirred at 1,000 rpm for 2 days at room temperature to ensure uniform distribution of materials. Once the paste is homogenous, it is cast onto the carbon sheet at a concentration of 0.003 g/cm^2. In setting up the three-electrode cell, the working electrode (the carbon sheet with the composite paste) is combined with two additional electrodes: a secondary electrode and a calomel electrode. The electrochemical measurements are carried out using a 1.0 M Na_2SO_4 electrolyte and a CHI608E electrochemical workstation. This device conducts electrochemical measurements by evaluating the current-voltage relationship to generate cyclic voltammetry over a potential range of 0.0–1.0 V. Additionally, it measures the time–voltage relationship through chronopotentiometry to determine the discharge time (Δt) and discharge voltage (ΔV). The C_S of the pseudo-supercapacitor is specified using the discharge data and the mass load of the paste, as defined by Eq. (1) [2]. This calculation provides a measure of the capacitor's ability to maintain charge.

To further assess the performance of the fabricated pseudo-supercapacitor, a Ragone plot is created. This plot illustrates the relationship between E and P, which are key indicators of a supercapacitor's efficiency. These values are derived using Eqs. (2) and (3) [3], respectively, which take into account the maximum and minimum voltage values observed during the electrochemical tests.

Overall, the described method ensures the creation of a high-performance pseudo-supercapacitor by utilizing the MnO_2-MnS/P2MA PN nanocomposite. The process includes

detailed steps to achieve a homogenous paste, careful casting onto the carbon sheet, and precise setup of the three-electrode cell for accurate electrochemical measurements. This comprehensive approach guarantees that the fabricated pseudo-supercapacitor exhibits optimal charge storage capabilities and efficiency, as demonstrated by the cyclic voltammetry curves, chronopotentiometry data, and the resulting Ragone plot (Figure 1).

$$C_S = I \cdot \Delta t / \Delta V \cdot m, \tag{1}$$

$$E = 0.5 C_S \times (V_{max}^2 - V_{min}^2), \tag{2}$$

$$P = E / \Delta t. \tag{3}$$

3 Results and discussion

3.1 Analyses

The characterization of the MnO_2-MnS/P2MA PN nanocomposite was carried out using FTIR analysis, as shown in Figure 2(a). This provides and helps confirm the incorporation of MnO_2-MnS into the polymer matrix by examining the functional groups present. For the pure P2MA polymer, the N–H and N–S stretching vibrations are observed at 3,373 cm^{-1}. However, in the PN nanocomposite, these peaks shift to 2,297 cm^{-1}, indicating the successful integration of MnO_2-MnS within the polymer structure.

A similar shift is observed for another vibrational mode, initially detected at 1,306 cm^{-1} in the P2MA polymer, which appears at 1,310 cm^{-1} in the nanocomposite. This change in the absorption band positions serves as a significant indicator of alterations in the molecular structure, specifically suggesting changes in the rotational dynamics of the ring groups due to the introduction of MnO_2 and MnS. These shifts in the FTIR spectra highlight the interaction between the polymer and the inserted metal oxide and sulfide, suggesting modifications in the chemical environment and structural arrangement of the composite material. The results confirm that the presence of MnO_2-MnS impacts the molecular vibrations, reflecting the successful formation of the PN nanocomposite and providing

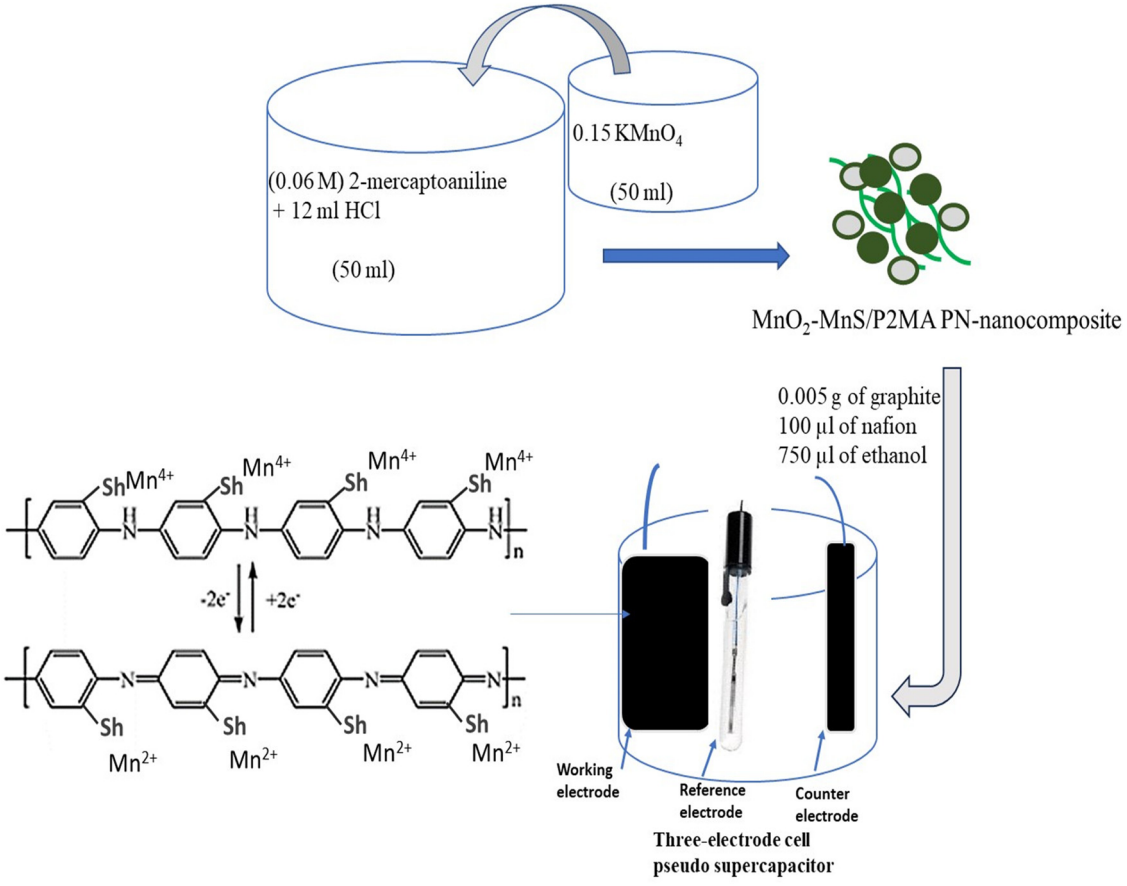

Figure 1: The single-step fabrication of the MnO_2-MnS/P2MA PN nanocomposite and the fabrication of the pseudo-supercapacitor.

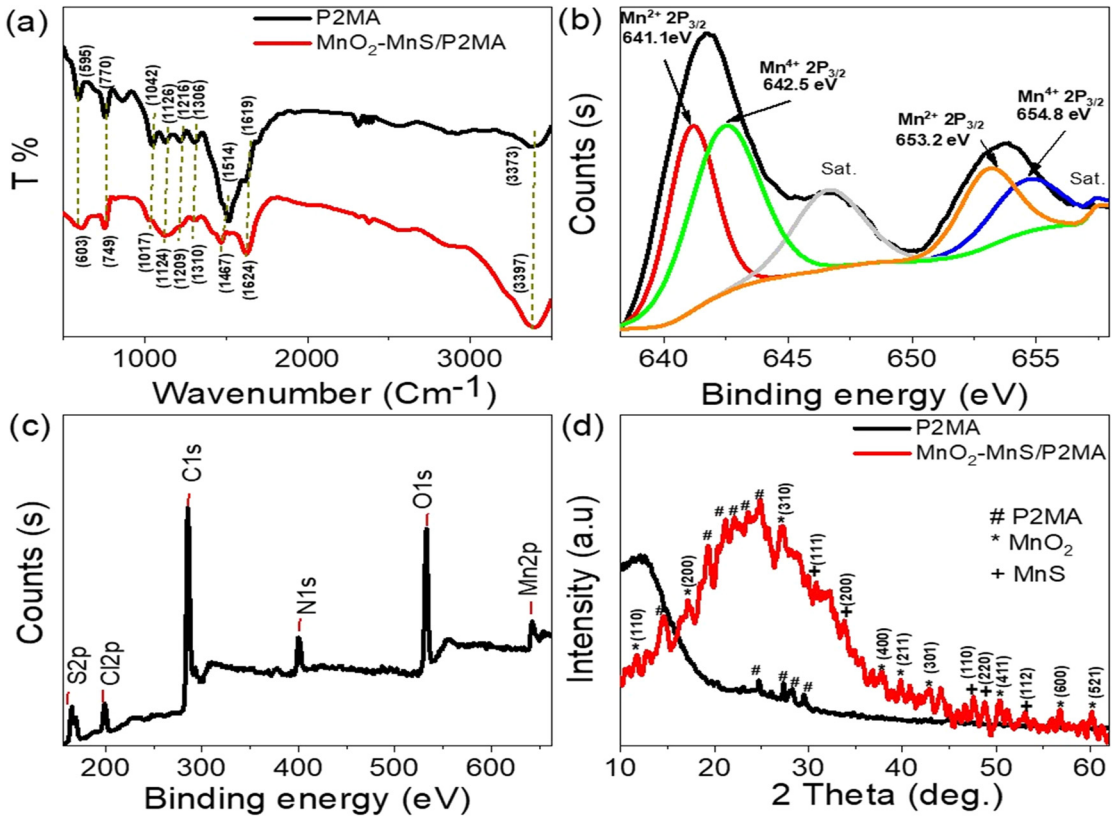

Figure 2: The chemical investigation of MnO_2-MnS/P2MA PN nanocomposite: (a) FTIR spectroscopy, (b) XPS Mn, (c) XPS survey, and (d) XRD pattern.

structural properties. Table 1 summarizes these groups' investigation of the composite relative to the monomer.

The chemical composition and oxidation states of the synthesized MnO_2-MnS/P2MA PN nanocomposite are evaluated using XPS analysis. As shown in Figure 2(b), the XPS analysis of the Mn element focuses on the 2p orbital, revealing binding energies corresponding to Mn^{2+} and Mn^{4+}, which are indicative of MnS and MnO_2, respectively. For Mn^{2+}, the binding energies are 641.1 and 653.2 eV for the $Mn2p_{3/2}$ and $Mn2p_{1/2}$ orbitals [25]. In contrast, Mn^{4+} exhibits binding energies at 642.5 and 654.8 eV for the same orbitals, respectively [26,28].

To further analyze the elemental structure of the MnO_2-MnS/P2MA PN nanocomposite, a comprehensive XPS survey was conducted, as shown in Figure 2(c), and identifies the presence of various elements within the composite. The binding energies detected for carbon (C), nitrogen (N), and sulfur (S) are 285.3, 401, and 165.8 eV, respectively. Additionally, O for the oxide components is observed at 532 eV, and chlorine (Cl), attributed to the acidic medium, is identified at 200 eV. These findings confirm the elemental constituents of the MnO_2-MnS/P2MA PN nanocomposite.

The detailed XPS analysis provides a crucial investigation into the chemical structure of the composite. The presence of Mn^{2+} and Mn^{4+} confirms the successful integration of MnS and MnO_2 within the P2MA matrix. The

Table 1: The FTIR analysis of functional groups in the MnO_2-MnS/P2MA PN nanocomposite compared to the pristine P2MA polymer

Band position (cm^{-1})		Group
MnO_2-MnS/P2MA PN nanocomposite	**P2MA**	
3,397	3,373	N–H [20] and S–H [21]
1,467 and 1,624	1,514 and 1,619	Ring C–C and C═C benzene [22]
1,310	1,306	C–N [23]
1,124 and 1,209	1,126 and 1,216	C–H [3]
749	770	C–H bending out of plane ortho-disubstituted [24]

identification of C, N, S, O, and Cl further substantiates the composite's composition and the interactions between the organic polymer and inorganic constituents. The observed binding energies align with the expected values for these elements and their respective oxidation states, indicating a well-defined composite structure. To further assess performance, the elemental composition of the composite was analyzed using XPD. The estimated percentages of C, O, N, Cl, S, and Mn are 61.54, 16.5, 7.86, 3.9, 8.94, and 1.26%, respectively. Overall, the XPS analysis effectively characterizes the MnO_2-MnS/P2MA PN nanocomposite, demonstrating the integration of the various components. The presence of Mn^{2+} and Mn^{4+} alongside other elements suggests a complex yet stable composite structure, suitable for applications in charge storage. The analysis confirms the chemical compatibility and integration of the materials, which is essential for optimizing the composite's electrochemical performance. The detailed understanding of the elemental composition and oxidation states provided by XPS analysis is instrumental in advancing the development and application of this nanocomposite in energy storage technologies.

To complete the chemical characterization of the MnO_2-MnS/P2MA PN nanocomposite, the crystalline behavior of these materials is analyzed using XRD patterns, as estimated in Figure 2(d). This analysis highlights a significant variation in the crystalline properties of the pristine polymer and the formed composite. After the formation of the composite, numerous peaks emerge, indicating a notable enhancement in the crystalline structure, which in turn suggests improved charge storage capabilities within the crystalline matrix of the composite.

For the MnO_2 inside the polymer network, the XRD peaks reflect the formation of the alpha phase, in which these peaks are observed at 11.6, 17.2, 27.2, 37.9, 40.8, 42.7, 44.1, 50.4, 56.7, and 60.2° corresponding to the growth directions (110), (310), (400), (211), (111), (301), (131), (411), (600), and (521), respectively, as per the JCPDS data (024-0735) [27,28]. Additionally, the MnS material within the composite shows characteristic peaks at 2θ values of 30.8, 33.9, 47.6, 48.8, and 53.2°, corresponding to the growth directions (111), (200), (110), (220), and (112), correspondingly [29,30].

The pristine P2MA exhibits four weak peaks, which denote its semi-crystalline nature. However, after the composite formation, six peaks emerge, reflecting a significant enhancement in its crystalline structure. This improvement in crystallinity is indicative of the enhanced charge storage potential of the composite material.

For the composite, The crystalline size is determined to be 42 nm, calculated by the Scherrer equation (Eq. (4)) [31], based on the high-intensity peak at 27.2°. This small crystalline size is beneficial for charge storage applications as it provides a larger area for electrochemical reactions, thereby enhancing the performance of the supercapacitor.

$$D = 0.9\lambda/\beta\cos\theta. \tag{4}$$

The topographical and morphological behaviors of MnO_2-MnS/P2MA PN nanocomposite were investigated using SEM, as estimated in Figure 3(a) and (b) at various magnifications. These images reveal the formation of a porous network, which is highly promising due to its substantial surface area and porosity, making it an excellent candidate for charge storage applications. The network is composed of small fibrous particles interconnected to form this porous structure.

Figure 3(d) provides a detailed view of this structure, showing how the network extends and connects to form a cohesive structure. The varying colors in the image, ranging from dark to faint, represent the inorganic and organic components within this composite, highlighting the integration of MnO_2 and MnS within the polymer matrix.

In contrast, the pristine P2MA exhibits a different morphology characterized by spherical particles. These larger particles are made up of smaller granules that aggregate to form the larger spheres. The presence of a porous structure within these spherical particles facilitates the incorporation of other materials during composite formation processes, enhancing their functionality in various applications.

So, the SEM analysis confirms that the MnO_2-MnS/P2MA PN nanocomposite possesses a highly porous and interconnected structure, which is advantageous for enhancing charge storage capacity. This morphology, combined with the compositional elements of MnO_2 and MnS, contributes to the improved electrochemical composite behavior.

3.2 The electrochemical testing of the synthesized MnO_2-MnS/P2MA PN nanocomposite pseudo-supercapacitor

The synthesized MnO_2-MnS/P2MA PN nanocomposite pseudo-supercapacitor exhibits electrochemical charge storage properties primarily through redox reactions. The charge storage process involves the reduction reaction, where the composite materials store and accumulate charges, followed by the oxidation reaction, which facilitates the de-insertion of these charges. This behavior is attributable to the redox capabilities of the materials within the composite, including MnO_2, MnS, and P2MA. Specifically, manganese (Mn) undergoes reduction to Mn^{2+} and subsequent oxidation to Mn^{4+}, while P2MA transitions from a benzene-like structure to a quinoid structure through similar redox processes.

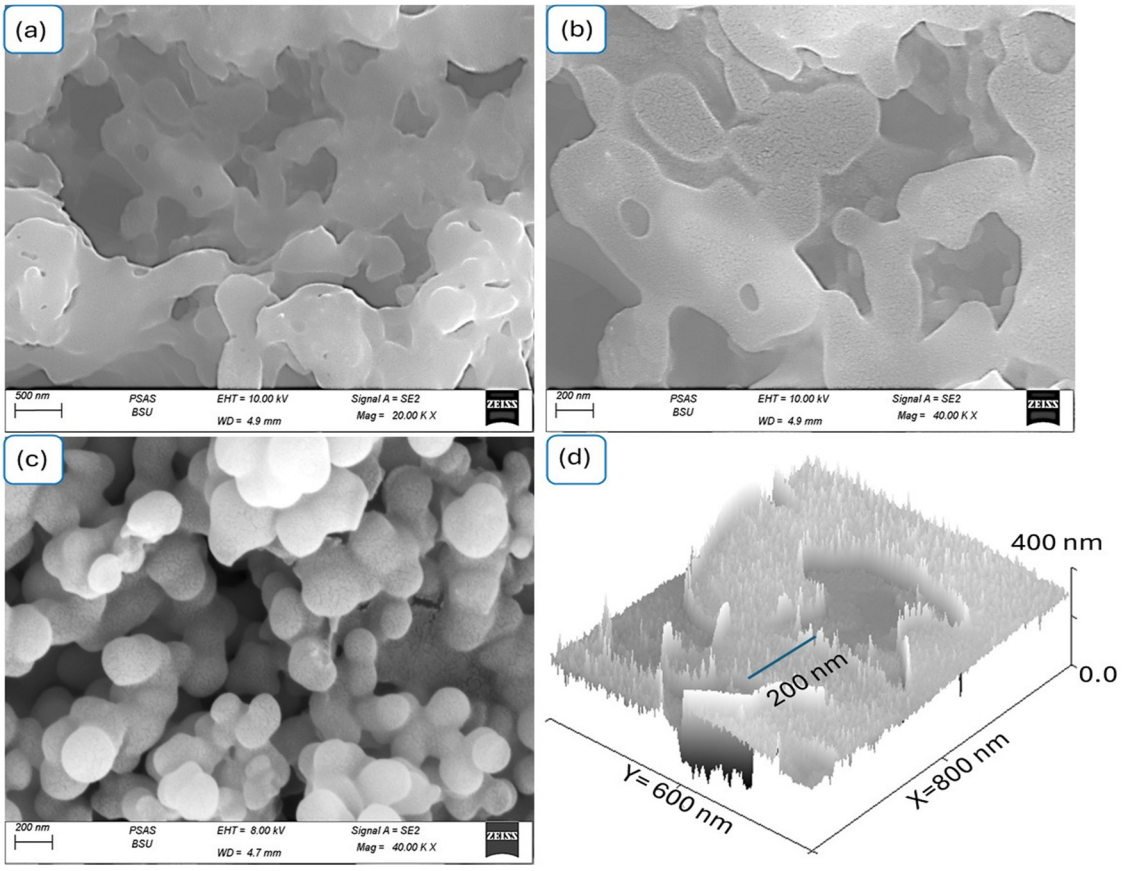

Figure 3: (a and b) SEM of the synthesized MnO$_2$-MnS/P2MA PN nanocomposite at various magnifications and (d) cross section for this composite. (c) SEM of P2MA.

Figure 4 provides a clear illustration of this phenomenon. In Figure 4(a), the electrochemical reactions of charge and discharge are depicted, showing a significant dependence on the current densities applied. As the current decreases, the discharge time notably increases, with optimal values recorded at 0.6 and 1.0 A/g, corresponding to discharge times of 80 and 34 s, respectively.

Additionally, Figure 4(b) presents cyclic voltammetry data, highlighting pronounced peaks in both positive and negative directions, with substantial areas under the

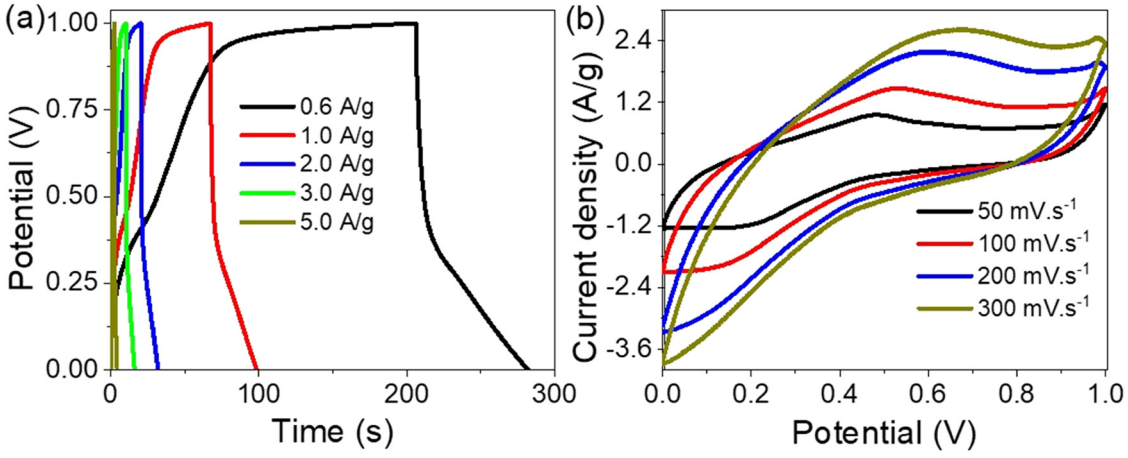

Figure 4: (a) Electrochemical discharge characteristics and (b) cyclic voltammetry for MnO$_2$-MnS/P2MA PN nanocomposite pseudo-supercapacitor.

curve. This area indicates robust charge storage capabilities, which are enhanced as the scan rate changes from 50 to 300 mV/s. The sharper peaks and larger areas under the curve correspond to increased current densities, estimating the composite's excellent charge storage performance.

The enhanced charge storage is largely due to the inclusion and de-insertion of H^+ ions from the acidic medium, which induce significant polarization in the P2MA acid. This polarization improves the conductivity and subsequently the charge storage within the porous structure of the MnO_2-MnS/P2MA PN nanocomposite. The promising nature of this composite is evident in its ability to efficiently store charge, making it a potential candidate for advanced supercapacitor applications.

The charge storage capability of the fabricated MnO_2-MnS/P2MA PN nanocomposite pseudo-supercapacitor is assessed through redox reactions involving charge insertion and subsequent charge de-insertion, as shown in Figure 5(a) based on C_S estimation. The maximum C_S values of 120 and 86 F/g are achieved at 0.6 and 1.0 A/g, respectively, illustrating the effect of current on the supercapacitor's charge storage behavior. Lower current values facilitate a more orderly insertion of charge during the redox reactions, resulting in a longer discharge time. This behavior is described by Eq. (1), which relates the mass loaded (Δm), discharge time (Δt), and discharge voltage (ΔV). By combining these factors, the C_S value is effectively determined, with the highest value corresponding to the discharge time of a longer value at a lower current density.

The estimation of the energy (E) value is demonstrated in Figure 5(b) based on Eq. (2), considering the squared values of the voltages relative to the C_S values. The optimal E values are found at lower current densities, with values

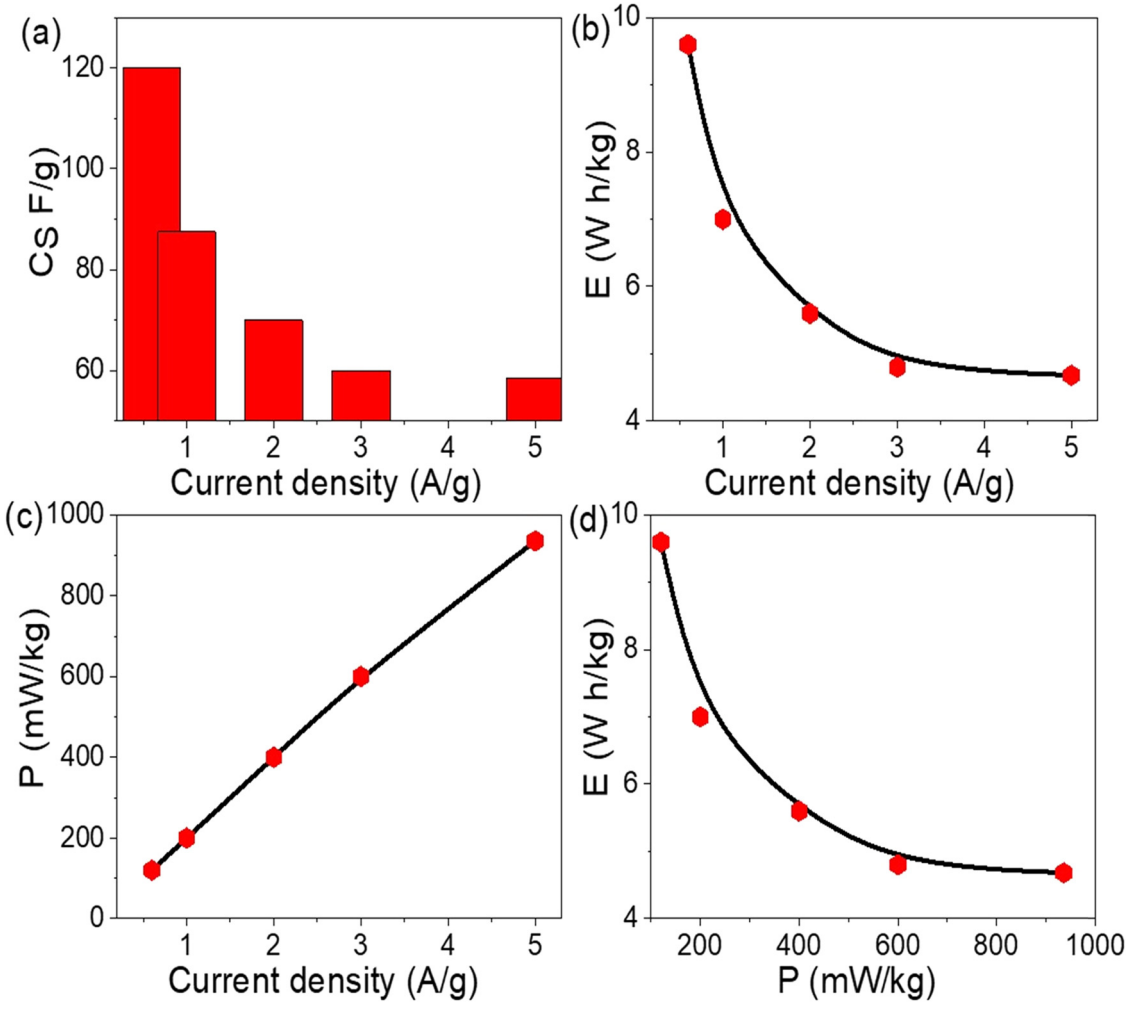

Figure 5: The evaluated charge storage behavior through the evaluated parameters: (a) C_S, (b) E, (c) P, and (d) Ragone plot for MnO_2-MnS/P2MA PN nanocomposite pseudo-supercapacitor.

Table 2: The charge storage performance of the MnO_2-MnS/P2MA PN nanocomposite relative to other literature

Supercapacitor electrode	C_S (F/g)	Current density (A/g)	Electrolyte
MnO_2-Mn_2O_3/poly-2-methyl aniline [4]	72	0.2	1.0 M Na_2SO_4
Polypyrrole-Ni$(OH)_2$ [33]	70	0.005	poly(vinyl alcohol)/H_3PO_4
MnO_2-MnS/G-C3N4 [34]	44	0.2	1.0 M Na_2SO_4
Polyaniline/silver oxide/silver [35]	4.0	0.2	1 M NaOH
Gd/graphitic material [36]	16	—	Poly(vinyl alcohol)/H_3PO_4
β-Ni$(OH)_2$/G-C3N4 [13]	20.5	1	1 M NaOH
CoO-CuO/G-C3N4 [37]	65	0.5	6 M KOH
Zn$(OH)_2$ [38]	100	0.2	2 M KOH
MnO_2-MnS/P2MA (this work)	120	0.6	1.0 M Na_2SO_4

of 9.7 and 7.0 W h/kg at 0.6 and 1.0 A/g, respectively. These high energy values highlight the ability of the fabricated supercapacitor to store substantial energy in a compact and lightweight MnO2-MnS/P2MA PN nanocomposite.

Figure 5(c) illustrates the estimation of the output power (P) using Eq. (3), in relation to the discharge time (Δt). The optimal P values increase with the applied current, reaching approximately 960 mW/kg. This indicates the supercapacitor's capability to deliver significant power to an external source, relative to the mass of the MnO2-MnS/P2MA PN nanocomposite. The Ragone plot [32] in Figure 5(d) is used to estimate both P and E values, showing the relationship between stored energy and produced power. According to the plot, the stored energy decreases sequentially with increasing power output. This relationship allows for an effective evaluation of the stored and discharged energies of the supercapacitor. Then, the MnO_2-MnS/P2MA PN nanocomposite pseudo-supercapacitor demonstrates excellent charge storage through redox reactions, influenced by current density. With a great behavior relative to the other previous studies as shown in Table 2.

The evaluation of charge storage in the fabricated MnO_2-MnS/P2MA PN nanocomposite pseudo-supercapacitor can be assessed through the charge transfer between the composite paste and the electrode. The effectiveness of this charge transfer, which determines the supercapacitor's charge storage capacity, is illustrated in the Nyquist plot shown in Figure 6(a). The solution resistance (R_S), measured at 7.3 Ω, reflects the resistance encountered by the charge passing through the solution and the composite paste. Additionally, the charge transfer resistance (R_{CT}) associated with the semicircle in the Nyquist plot is measured at 20.3 Ω. These values indicate excellent charge transfer capabilities for the supercapacitor, facilitated by the materials' inherent properties. The impedance values, derived using the Randle circuit depicted in the figure, underscore the efficiency of the MnO_2, MnS, and P2MA

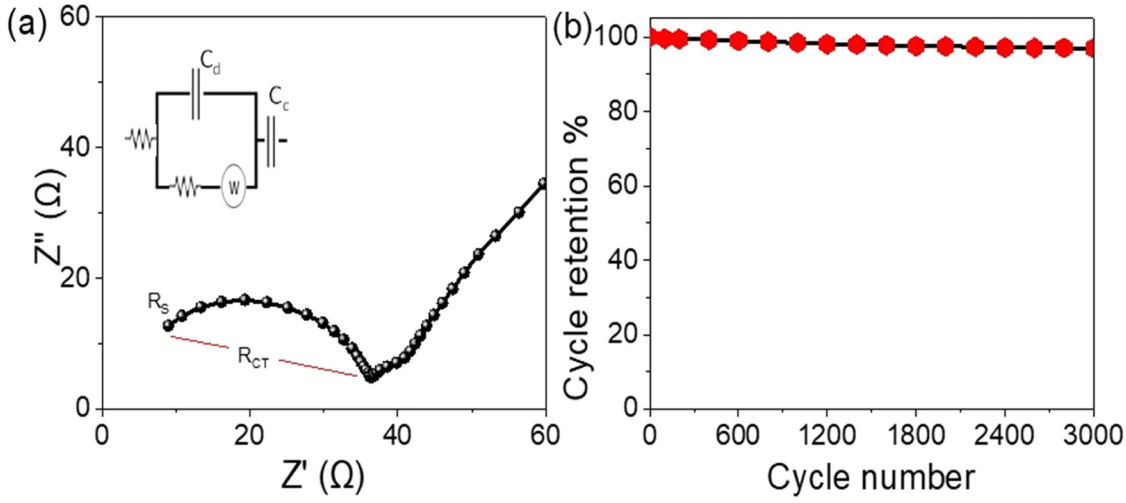

Figure 6: (a) The evaluation of the charge transfer inside the MnO_2-MnS/P2MA PN nanocomposite and (b) the cycle retention.

components, which possess significant semiconductive properties. These materials enable efficient charge transfer due to their superior semiconductivity. Figure 6(b) illustrates the cycling stability of the supercapacitor, showing an impressive retention of 99.2% after 1,000 cycles, which gradually declines to 97% after 3,000 cycles. This high stability indicates the MnO_2-MnS/P2MA PN nanocomposite pseudo-supercapacitor's potential for commercial applications, combining efficiency with cost-effectiveness and scalability for mass production.

4 Conclusions

The MnO_2-MnS/P2MA PN composite is fabricated using a single-step process. SEM analysis reveals a nanoscale network formation that merges to create an extensive surface area, while XRD analysis shows distinct crystalline peaks, indicating excellent semiconductive properties with a crystalline size of 42 nm. This nanocomposite is used as a working electrode in a three-electrode cell setup to evaluate its charge storage capabilities electrochemically. At lower current densities, the optimal *E*-values are achieved, with 9.7 W h/kg at 0.6 A/g and 7.0 W h/kg at 1.0 A/g. The C_S also reaches its peak within this current density range, with values of 120 and 86 F/g, correspondingly. The EIS shows notable performance with an R_s value of 7.3 Ω and an impressive cycle retention rate of 99.2% over 1,000 cycles.

The combination of a simple one-pot fabrication process, excellent charge storage performance, and high stability highlight the nanocomposite for charge storage applications. The MnO_2-MnS/P2MA nanocomposite demonstrates superior EIS behavior, optimal energy and capacitance values, and remarkable cycle stability, reflecting its efficiency and reliability for charge storage solutions.

Acknowledgments: Ongoing Research Funding program, (ORF-2025-845), King Saud University, Riyadh, Saudi Arabia.

Funding information: Ongoing Research Funding program, (ORF-2025-845), King Saud University, Riyadh, Saudi Arabia.

Author contributions: Mohamed Rabia: experimental, analysis, and writing. Eman Aldosari: writing, supervision, and project funding. Qinfang Zhang: revision and supervision. Hissah Hamad Altilasi: writing and supervision. All authors have accepted responsibility for the entire content of this manuscript and approved its submission.

Conflict of interest: The authors state no conflict of interest.

Data availability statement: All data generated or analyzed during this study are included in this published article.

References

[1] Pujari RB, Lokhande VC, Kumbhar VS, Chodankar NR, Lokhande CD. Hexagonal microrods architectured MoO_3 thin film for supercapacitor application. J Mater Sci: Mater Electron. 2016;27:3312–7.

[2] Rabia M, Abdallah Alnuwaiser M, Hasan F, Adel A. Abdelazeez A. Highly wrinkled porous polypyrrole for the enhancement of the performance of an Fe_2S_3-Fe_2O_3/poly-O-amino benzenethiol supercapacitor from a basic medium. Inorganics. 2023;11:402.

[3] Elsayed AM, Abdallah Alnuwaiser M, Rabia M. Effect of brain-like shape polypyrrole nanomaterial on the capacitance and stability enhancements of β-Ni(OH)2 two-symmetric electrodes supercapacitor. J Mater Sci: Mater Electron. 2023;34:1–10.

[4] Alkallas FH, Elsayed AM, Trabelsi ABG, Rabia M. Basic and acidic electrolyte mediums impact on MnO_2-Mn_2O_3/poly-2-methylaniline hexagonal nanocomposite pseudo-supercapacitor. Phys Scr. 2024;99:065972.

[5] Karimzadeh Z, Shokri B, Morsali A. Rapid cold plasma synthesis of cobalt metal–organic framework/reduced graphene oxide nanocomposites for use as supercapacitor electrodes. Sci Rep. 2023;13(1):1–11.

[6] Alshammari DA, Ahmed IA, Alahmari SD, Abdullah M, Aman S, Ahmad N, et al. Electrochemical investigation of niobium doped nickel selenide nanostructure for supercapacitor devices. J Energy Storage. 2024;75:109886.

[7] Adriyani TR, Ensafi AA, Rezaei B. Flexible and sewable electrode based on Ni-Co@PANI-salphen composite-coated on textiles for wearable supercapacitor. Sci Rep. 2023;13(1):1–13.

[8] Ramadoss J, Sonachalam A, Govindasamy M. Surface modification effect on V-doped Ti3C2Tx as bifunctional catalyst electrodes for symmetric supercapacitor and the hydrogen evolution reaction. Energy Fuels. 2023;37:17561–74.

[9] Alshammari DA, Aman S, Ahmad N, Riyad YM, Tahir Farid HM. Development of N doped C/$MnAl_2O_4$ spinel as environmental friendly energy storage devices. Ceram Int. 2024;50:5424–33.

[10] AlAnazi M, Ghrib T, Ercan F, Alsubaie M, Demirci T, Kaygili O, et al. Structural, optical, and electrical investigation of multilayered MnO2(n)/NiO(p) heterojunctions for supercapacitors applications. Surf Interfaces. 2023;42:103321.

[11] Kulandaivalu S, Suhaimi N, Sulaiman Y. Unveiling high specific energy supercapacitor from layer-by-layer assembled polypyrrole/graphene oxide|polypyrrole/manganese oxide electrode material. Sci Rep. 2019;9(1):1–10.

[12] Lu T, Zhang Y, Li H, Pan L, Li Y, Sun Z. Electrochemical behaviors of graphene–ZnO and graphene–SnO_2 composite films for supercapacitors. Electrochim Acta. 2010;55:4170–3.
[13] Roshni CP, Jithesh K, Manuraj M, Govind Raj K, Rakhi RB. β-Ni(OH)2 supported over g-C3N4: A novel catalyst for para-nitrophenol reduction and supercapacitor electrode. Results Chem. 2022;4:100498.
[14] Avinash B, Ravikumar CR, Kumar MRA, Santosh MS, Pratapkumar C, Nagaswarupa HP, et al. NiO bio-composite materials: Photocatalytic, electrochemical and supercapacitor applications. Appl Surf Sci Adv. 2021;3:100049.
[15] Kumar MRA, Abebe B, Nagaswarupa HP, Murthy HCA, Ravikumar CR, Sabir FK. Enhanced photocatalytic and electrochemical performance of TiO_2-Fe_2O_3 nanocomposite: Its applications in dye decolorization and as supercapacitors. Sci Rep. 2020;10(1):1–15.
[16] Afza N, Shivakumar MS, Alam MW, Kumar AN, Bhatt AS, Murthy HCA, et al. Facile hydrothermal synthesis of cerium oxide/rGO nanocomposite for photocatalytic and supercapacitor applications. Appl Surf Sci Adv. 2022;11:100307.
[17] Kedir CN, Salinas-Torres D, Quintero-Jaime AF, Benyoucef A, Morallon E. Hydrogels obtained from aniline and piperazine: Synthesis, characterization and their application in hybrid supercapacitors. J Mol Struct. 2022;1248:131445.
[18] Zang L, Liu Q, Qiu J, Yang C, Wei C, Liu C, et al. Design and fabrication of an all-solid-state polymer supercapacitor with highly mechanical flexibility based on polypyrrole hydrogel. ACS Appl Mater Interfaces. 2017;9:33941–7.
[19] Li J, Yan W, Zhang G, Sun R, Ho D. Natively stretchable micro-supercapacitors based on a PEDOT:PSS hydrogel. J Mater Chem C. 2021;9:1685–92.
[20] Zaki SE, Basyooni MA, Shaban M, Rabia M, Eker YR, Attia GF, et al. Role of oxygen vacancies in vanadium oxide and oxygen functional groups in graphene oxide for room temperature CO_2 gas sensors. Sens Actuators, A: Phys. 2019;294:17–24.
[21] Azzam EMS, Abd El-Salam HM, Aboad RS. Kinetic preparation and antibacterial activity of nanocrystalline poly(2-aminothiophenol). Polym Bull. 2019;76:1929–47.
[22] Alkallas FH, Elsayed AM, Trabelsi ABG, Rabia M. Porous-spherical MnO_2-$Mn(OH)_2$/polypyrrole nanocomposite thin film photodetector in a wide optical range from UV to IR. Opt Quantum Electron. 2023;55:1078.
[23] Alkallas FH, Elsayed AM, Trabelsi ABG, Rabia M. Quantum dot supernova-like-shaped arsenic (III) sulfide-oxide/polypyrrole thin film for optoelectronic applications in a wide optical range from ultraviolet to infrared. Catalysts. 2023;13:1274.
[24] Elsayed AM, Alkallas FH, Trabelsi ABG, Rabia M. Highly uniform spherical MoO_2-MoO_3/polypyrrole core-shell nanocomposite as an optoelectronic photodetector in UV, Vis, and IR domains. Micromachines. 2023;14:1694.
[25] Cao X, Li H, He J, Kang L, Jiang R, Shi F, et al. Preparation and formation process of α-MnS@MoS2 microcubes with hierarchical core/shell structure. J Colloid Interface Sci. 2017;507:18–26.
[26] Chen K, Wang M, Li G, He Q, Liu J, Li F. Spherical α-MnO_2 supported on N-KB as efficient electrocatalyst for oxygen reduction in Al-air battery. Materials. 2018;11:601.
[27] Sannasi V, Subbian K. Influence of Moringa oleifera gum on two polymorphs synthesis of MnO_2 and evaluation of the pseudo-capacitance activity. J Mater Sci: Mater Electron. 2020;31:17120–32.
[28] Shah HU, Wang F, Javed MS, Ahmad MA, Saleem M, Zhan J, et al. In-situ growth of MnO_2 nanorods forest on carbon textile as efficient electrode material for supercapacitors. J Energy Storage. 2018;17:318–26.
[29] Xu D, Jiao R, Sun Y, Sun D, Zhang X, Zeng S, et al. L-cysteine-assisted synthesis of urchin-like γ-MnS and its lithium storage properties. Nanoscale Res Lett. 2016;11:444.
[30] Mi L, Chen Y, Zheng Z, Hou H, Chen W, Cui S. Beneficial metal ion insertion into dandelion-like MnS with enhanced catalytic performance and genetic morphology. RSC Adv. 2014;4:19257–65.
[31] Ahmed AM, Rabia M, Shaban M. The structure and photoelectrochemical activity of Cr-doped PbS thin films grown by chemical bath deposition. RSC Adv. 2020;10:14458–70.
[32] Huo P, Ni S, Hou P, Xun Z, Liu Y, Gu J. A crosslinked soybean protein isolate gel polymer electrolyte based on neutral aqueous electrolyte for a high-energy-density supercapacitor. Polymers. 2019;11(5):863.
[33] Scarabelot LT, Muller D, de Souza LV, Hotza D, Rambo CR. $Ni(OH)_2$ aerogels incorporated with polypyrrole as electrodes for supercapacitors. J Electron Mater. 2017;46:5232–9.
[34] Ben Gouider Trabelsi A, Elsayed AM, Alkallas FH, Rabia M. Highly uniform nanocomposite through the decoration of MnS on graphitic carbon nitride as electrodes for symmetric supercapacitor. Phys Scr. 2023;98:116005.
[35] Atta A, Abdelhamied MM, Essam D, Shaban M, Alshammari AH, Rabia M. Structural and physical properties of polyaniline/silver oxide/silver nanocomposite electrode for supercapacitor applications. Int J Energy Res. 2022;46:6702–10.
[36] Kumar Kuila S, Ghorai A, Midya A, Sekhar Tiwary C, Kumar Kundu T. Chemisorption of gadolinium ions on 2D-graphitic carbon nitride nanosheet for enhanced solid-state supercapacitor performance. Chem Phys Lett. 2022;796:139572.
[37] Santos RS, Suresh Babu R, Devendiran M, Haddad DB, de Barros ALF. Facile synthesis of transition metal (M = Cu, Co) oxide grafted graphitic carbon nitride nanosheets for high performance asymmetric supercapacitors. Mater Lett. 2022;308:131156.
[38] Sasirekha C, Arumugam S. Electrochemical performance of zinchydroxide Zn(OH)2 nanosheet for supercapacitor application. AIP Conf Proc. 2017;1832:050047.